Supplemental Materials:

1) **Materials and Methods**
2) **Supplemental Figures**
3) **Supplemental Table Legends**
4) **Author Contributions**
5) **Supplemental Acknowledgements**

Materials and Methods:

Primary HSPC Isolation, Viral Transduction, *In Vitro* self-renewal, Flow Cytometry, ChIP, and RNA analysis.

Mice were euthanized in accordance with Medical College of Wisconsin Institutional Animal Care and Use Committee guidelines (IACUC# AUA2688). HSPCs were isolated from both male and female animals during the study. No animals or biological replicates were excluded from the analyses. HSPC isolations and viral transductions were performed as previously described{Milanovich:2015dt}. Lentiviral shRNAs used in this study came from the TRC consortium: *Rad21*-shRNA (shRNA1: TRCN0000174832; shRNA2: TRCN000017684), *Hoxa9*-shRNA (shRNA1: TRCN0000012510; shRNA2: TRCN0000012508) *Hoxa7*-shRNA (shRNA1: TRCN0000225923; shRNA2: TRCN0000218002), *Ctcf*-shRNA (shRNA1: TRCN0000039019; shRNA2: TRCN20000039022) or empty vector constructs (pLKO.1). To maintain selection, 1 ug/mL of puromycin and 100 ug/mL of hygromycin was used in methylcellulose culture. Methocult, RNA isolation, real-time PCR, Chromatin immunoprecipitation (ChIP), and Flow Cytometry was performed as in{Milanovich:2015dt, Pulakanti:2013jx, Stelloh:2016dy}. Two independent investigators performed assessment of colony forming units. Primers used in gene expression studies are shown in Table S1.

Immunoprecipitation:

32-D murine immortalized myeloblast cells were collected and washed with ice cold PBS. Cells were suspended in IP lysis buffer (Thermofisher Scientific Cat# 87787) containing PMSF and protease inhibitor cocktail. Whole cell lysates were isolated and 2000 µg of protein was used for immunoprecipitations. Immunoprecipitations were performed as previously described {Zhang:2008be}. Briefly, samples were suspended in 1200 µL of IP lysis buffer and precleared with 50 µL of Protein G PLUS-Agarose beads (Santa Cruz Biotechnology, Cat# sc-2002) and 1 ug normal mouse IgG antibody (Santa Cruz Biotechnology, Cat# sc-2025) for 1 hour at 4°C. 10 ug of antibodies or IgG were then added to the lysates and they were incubated at 4°C for 2 hours. 50uL of beads were then added to the lysates and rotated overnight at 4°C. The following morning, agarose beads were washed 5 times with 1 mL IP lysis buffer. Antigens were eluted from the beads using SDS-Sample buffer (Boston BioProducts, Cat# BP-111R). Samples were boiled for 10 minutes at 95°C and spun for 3 minutes at 2500 RPM. Equal volumes of samples were run on 8% SDS-PAGE gels along with an input control, and the presence of RAD21 was evaluated using anti-RAD21 antibody (Abcam, Cat# ab992). 293T co-immunoprecipitations were performed as previously reported{Rao:2010do}. All immunoblotting was performed as previously{Milanovich:2015dt, Pulakanti:2013jx} Antibodies used for protein applications are summarized in Table S2.

DNA Content Determination:

Cells were collected, washed with bone marrow wash medium, and counted using a hemocytometer. Per sample, 500,000 cells were suspended in PBS and stained with propidium iodide (PI). Percentages of cells in each stage of the cell cycle were determined by flow cytometry using an Accuri C6 flow cytometer. Analysis was performed using FCS Express software. Statistical analyses were determined by Student's t-test (two tailed, unpaired).

Microarray:

RNA from cells at the end of primary plating where collected and isolated as above. Arrays were run for 2 biological replicates each of empty vector control, *Rad21*-shRNA1, and *Rad21*-shRNA2. Probes were generated and hybridized to Affymetrix Mouse 430A_2 chips. CEL files were normalized with RMA {Irizarry:2003ge} and subsequently processed using Genepattern{Reich:2006jy} and GSEA {Subramanian:2005jt} similar to our previous work using default parameters{Rao:2010do}. For identification of genes differentially expressed by *Hoxa9* overexpression, we downloaded and reanalyzed data from{Muntean:2010ir} (GSE 212299). Specific datasets used are listed in Table S3. All new microarray data have been deposited into the NCBI GEO omnibus (ID GSE76320).

Reanalysis of Cancer Genome Atlas datasets:

Data for all AML samples within the TCGA (https://tcga-data.nci.nih.gov/tcga/dataAccessMatrix.htm) were downloaded. Level 3 expression data and mutation identification were directly taken from TCGA. Statistical significance was determined using a Mann-Whitney U test.

RNA Sequencing Bioinformatics

RNA-seq data for cells infected with shRNAs to luciferase, *Rad21*, or *Smc3*{Mullenders:2015fi} (GSE 72368) were downloaded and reanalyzed as previously described{Pulakanti:2013jx} . Briefly, raw data were downloaded and aligned to the mouse genome (mm9) using TopHat, and FPKMs for well-annotated genes were assigned using CuffLinks{Trapnell:2012kp}. FPKMs for each gene are listed in Table S4.

Statistical Analyses

Statistical significance was determined by Student's t-test (two tailed, unpaired) for all figures except Figure 3C which was a Mann-Whitney test to account for the unequal variance between groups. The number of biological replicates is listed in the figure legend for each figure. Error bars in all bar graphs represents the standard error of the mean of biological replicates. Asterisks (*) represent p-values < 0.05 and crosses (ł) indicate p-values < 0.01.

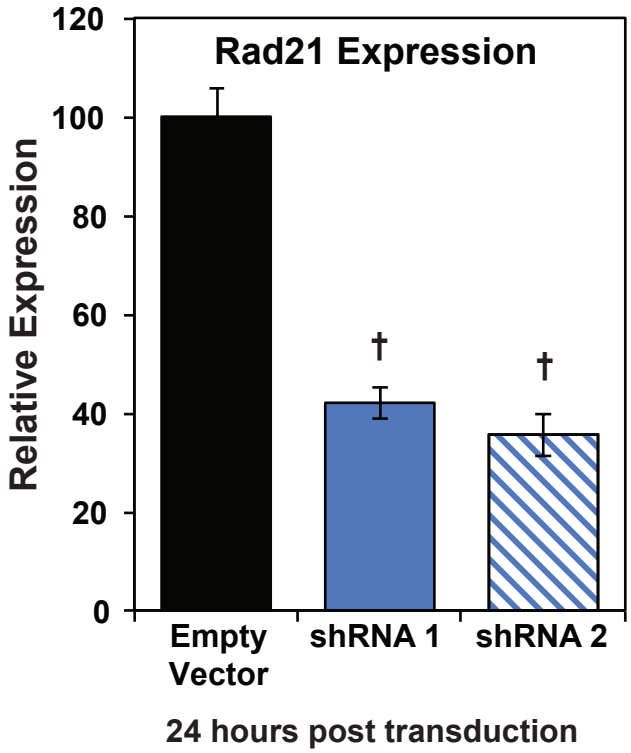
Rad21 Expression
Relative Expression
120
100
80
60
40
20
0
†
†
Empty Vector
shRNA 1
shRNA 2
24 hours post transduction

Figure S1. Lentiviral shRNA reduces *Rad21* levels in primary HSPCs. RT-qPCR analysis of primary HSPCs 24 hours after treatment with shRNA. Cells transduced with lentiviral shRNA were selected for 24 hours and RNA from puromycin-resistant cells was converted to cDNA, and analyzed using primers specific for *Rad21* mRNA. Each data point represents 7 independent biological replicates.

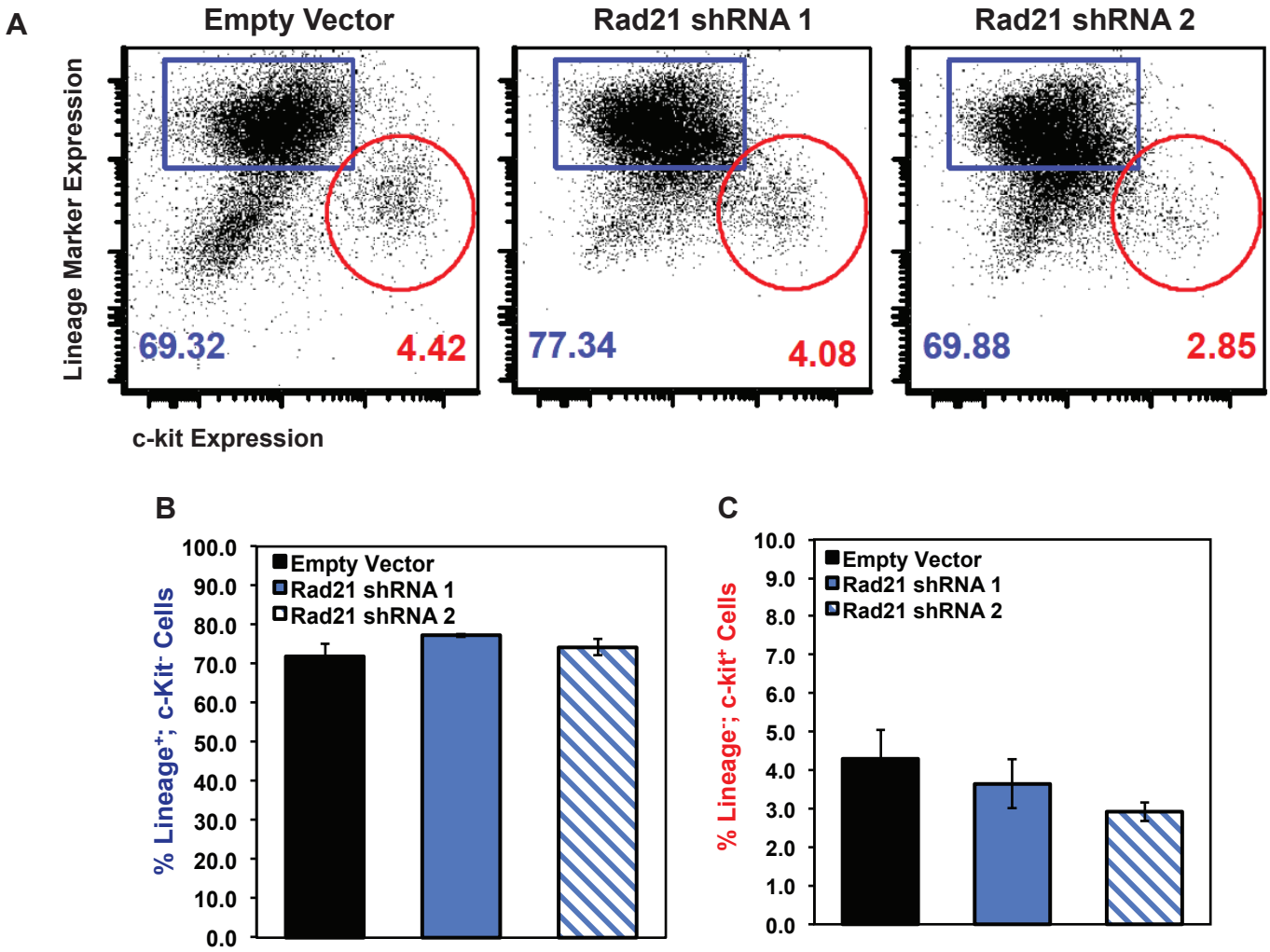
A
Empty Vector
Rad21 shRNA 1
Rad21 shRNA 2
Lineage Marker Expression
c-kit Expression
69.32
4.42
77.34
4.08
69.88
2.85
B
% Lineage+; c-Kit- Cells
Empty Vector
Rad21 shRNA 1
Rad21 shRNA 2
100.0
90.0
80.0
70.0
60.0
50.0
40.0
30.0
20.0
10.0
0.0
C
% Lineage-; c-kit+ Cells
Empty Vector
Rad21 shRNA 1
Rad21 shRNA 2
10.0
9.0
8.0
7.0
6.0
5.0
4.0
3.0
2.0
1.0
0.0

Figure S2. *Rad21* depletion does not selectively deplete HSPCs or differentiated lineages. (A) Representative flow cytometry dot plots of lineage marker (y-axis) vs c-kit (x-axis) performed on empty vector and *Rad21*-depleted HSPCs at the end of primary methylcellulose culture. (B) Bar graphs showing the percentages of c-kit-negative/lineage-positive averages from 3 independent biological replicates of the flow cytometry performed in A. (C) Bar graphs showing the percentages of c-kit-positive/lineage-negative averages from 3 independent biological replicates of the flow cytometry performed in A.

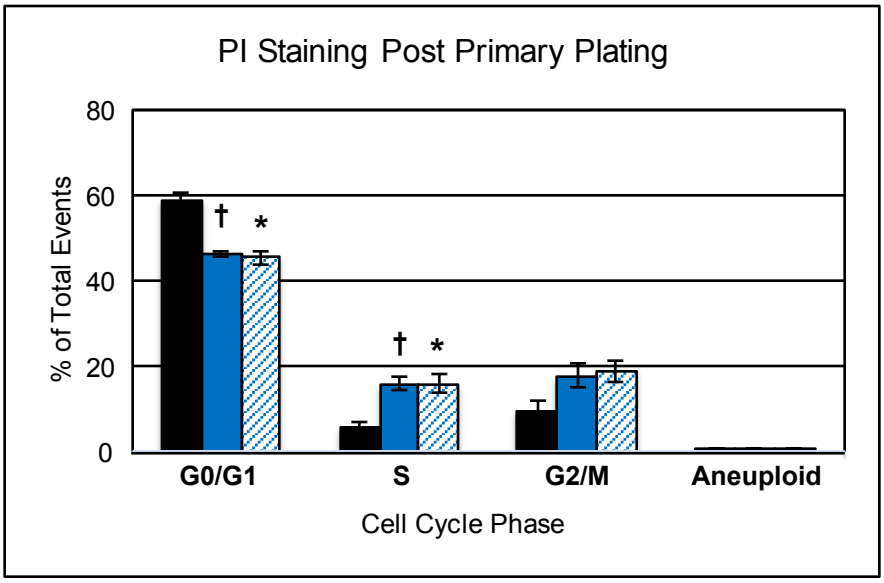
PI Staining Post Primary Plating
80
60
40
20
0
% of Total Events
†
*
†
*
G0/G1
S
G2/M
Aneuploid
Cell Cycle Phase

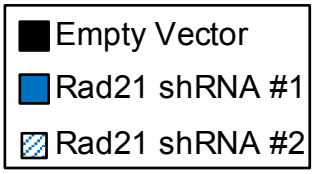
Empty Vector
Rad21 shRNA #1
Rad21 shRNA #2

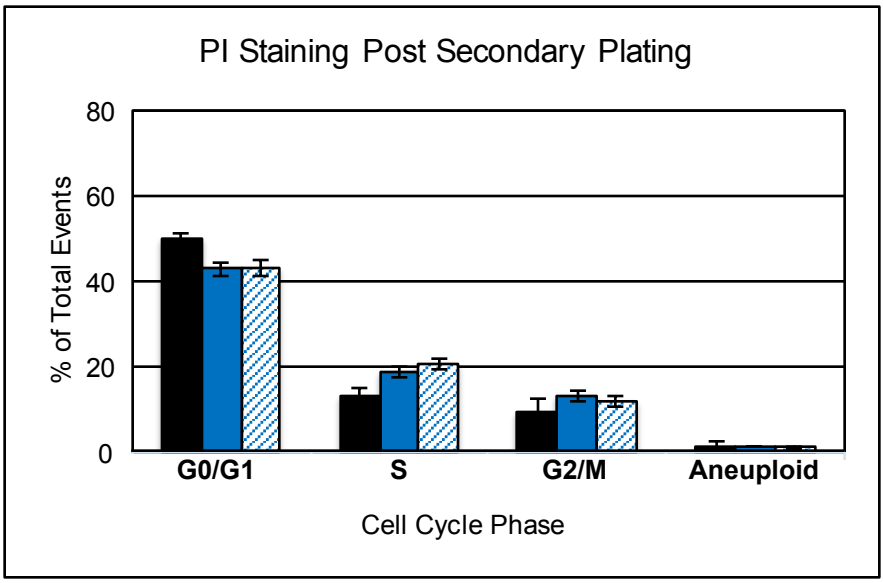
PI Staining Post Secondary Plating
80
60
40
20
0
% of Total Events
G0/G1
S
G2/M
Aneuploid
Cell Cycle Phase

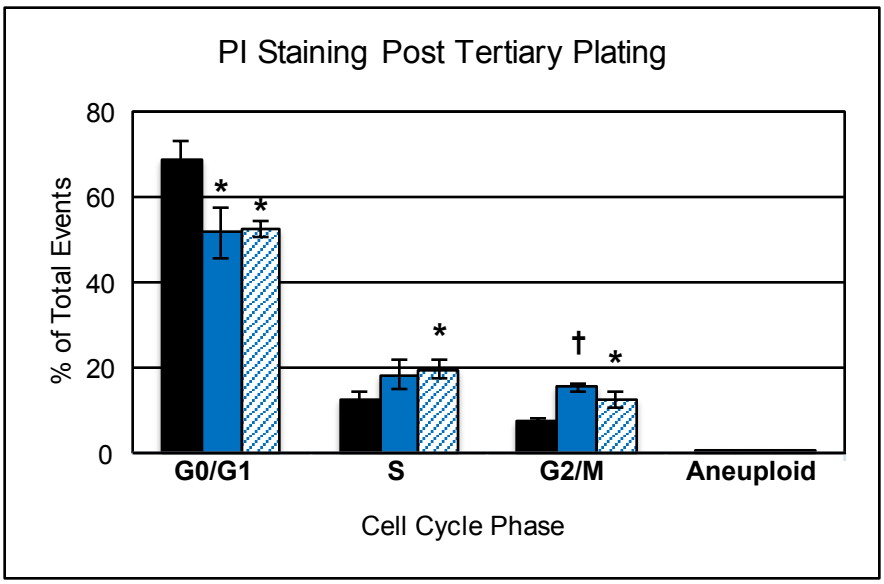
PI Staining Post Tertiary Plating
80
60
40
20
0
% of Total Events
*
*
*
†
*
G0/G1
S
G2/M
Aneuploid
Cell Cycle Phase

Figure S3. *Rad21* depletion alters cell cycle and does not induce aneuploidy. Flow cytometry of propidium iodide stained control and *Rad21*-shRNA1 and shRNA2 HSPCs at the end of primary, secondary, and tertiary methylcellulose passages. All data points represent 3 independent biological replicates.

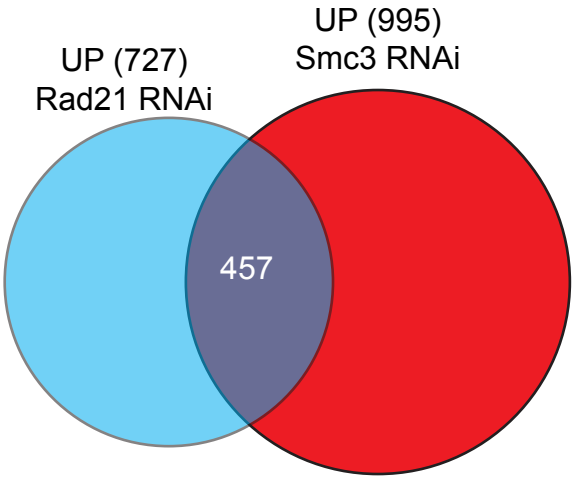
UP (727)
Rad21 RNAi
UP (995)
Smc3 RNAi
457

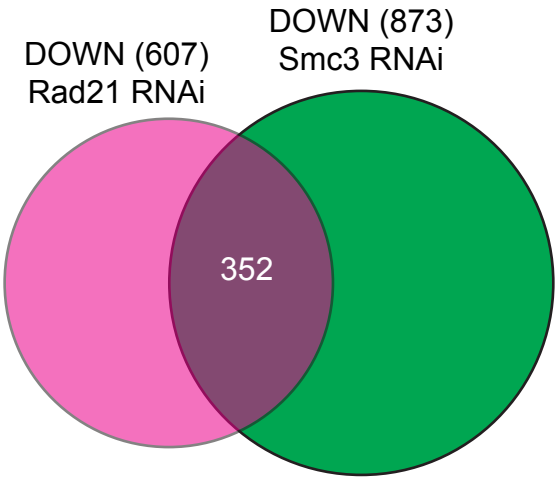
DOWN (607)
Rad21 RNAi
DOWN (873)
Smc3 RNAi
352

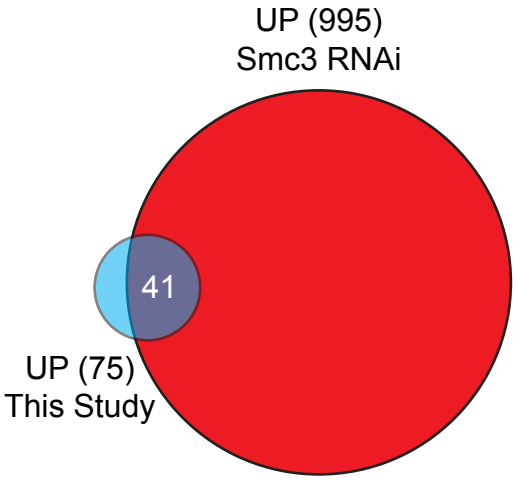
UP (995)
Smc3 RNAi
41
UP (75)
This Study

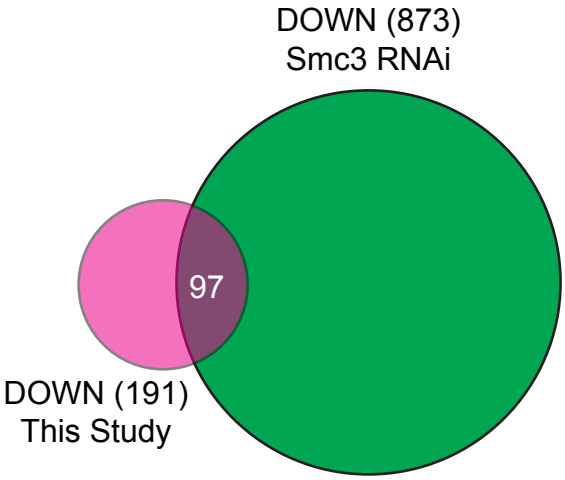
DOWN (873)
Smc3 RNAi
97
DOWN (191)
This Study

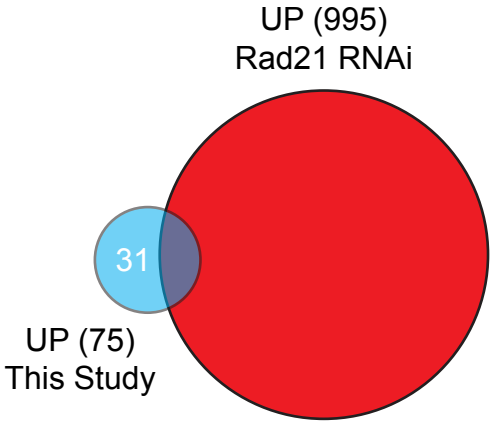
UP (995)
Rad21 RNAi
31
UP (75)
This Study

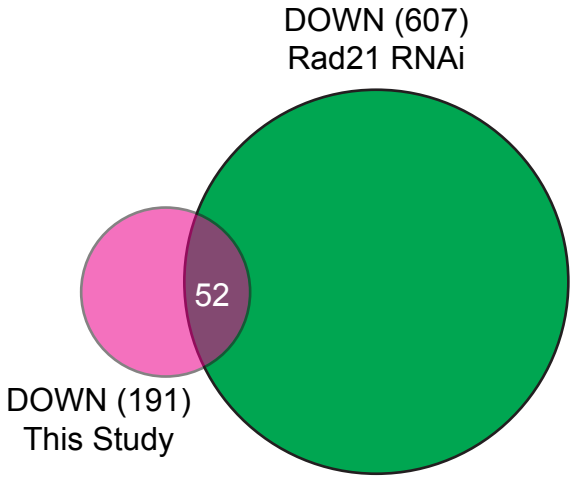
DOWN (607)
Rad21 RNAi
52
DOWN (191)
This Study

Figure S4. Overlap between transcriptome analyses of *Rad21*-depleted HSPCs vs previously published RNA-seq. Affected gene lists from *Rad21*-depleted HSPCs at the end of primary methylcellulose culture from our study and a previously published data set {Mullenders:2015fi}. Genes which showed significant changes (UP or DOWN) after *Rad21* depletion from this study (list of genes are shown in Table S5). For comparison, we used a similar fold-change for RNA-seq in which either *Rad21* or *Smc3* were depleted by RNAi (list of genes are shown in Table S4 {Mullenders:2015fi}). The number of genes in each list is shown in parentheses, and the size of each circle is proportional to the # of genes. Overlap between different gene sets is shown. Non-overlapping genes are likely secondary to subtle changes in the experimental conditions (differences in shRNA knockdown efficiency).

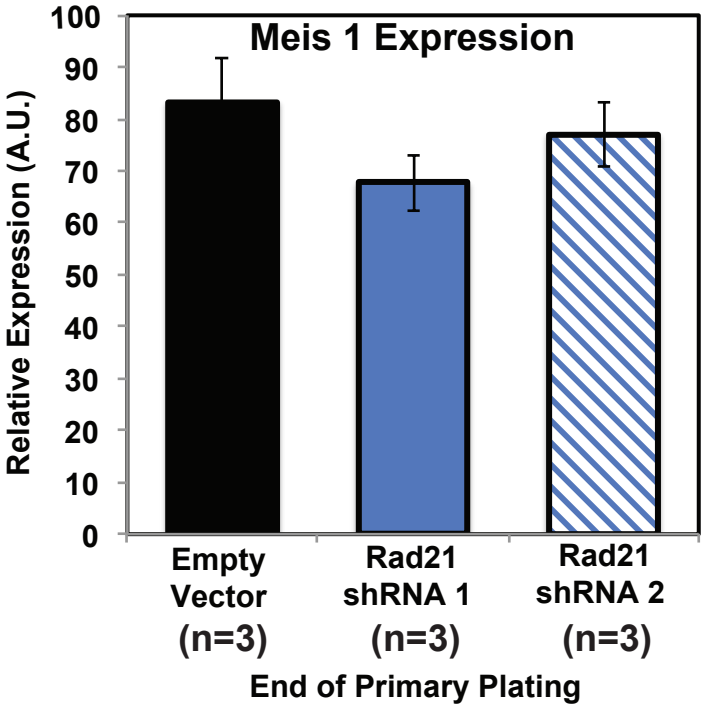
Meis 1 Expression
Relative Expression (A.U.)
100
90
80
70
60
50
40
30
20
10
0
Empty Vector (n=3)
Rad21 shRNA 1 (n=3)
Rad21 shRNA 2 (n=3)
End of Primary Plating

Figure S5. *Rad21* depletion does not affect *Meis1* expression. RT-qPCR results showing expression of *Meis1* in post primary methylcellulose culture *Rad21*-depleted or empty vector treated HSPCs.

A

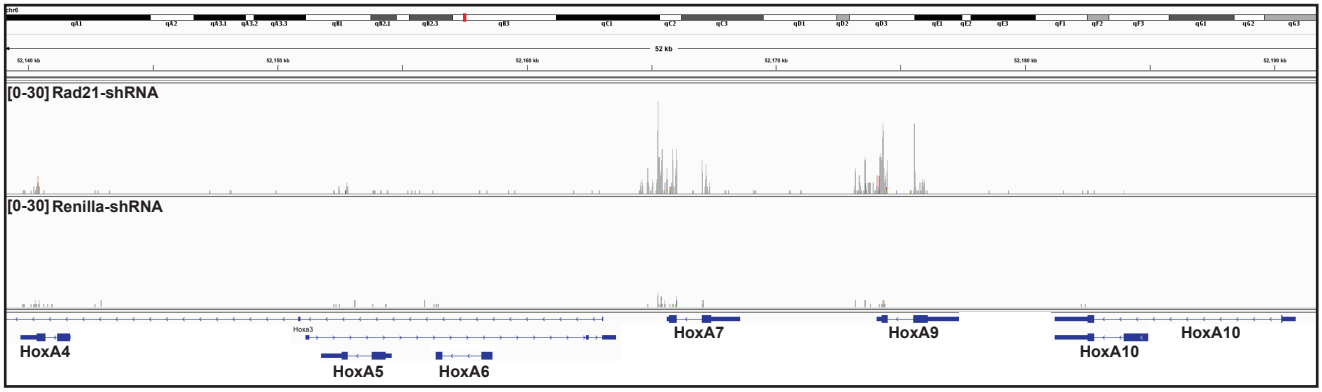
[0-30] Rad21-shRNA
[0-30] Renilla-shRNA
HoxA4
HoxA5
HoxA6
HoxA7
HoxA9
HoxA10
HoxA10

B

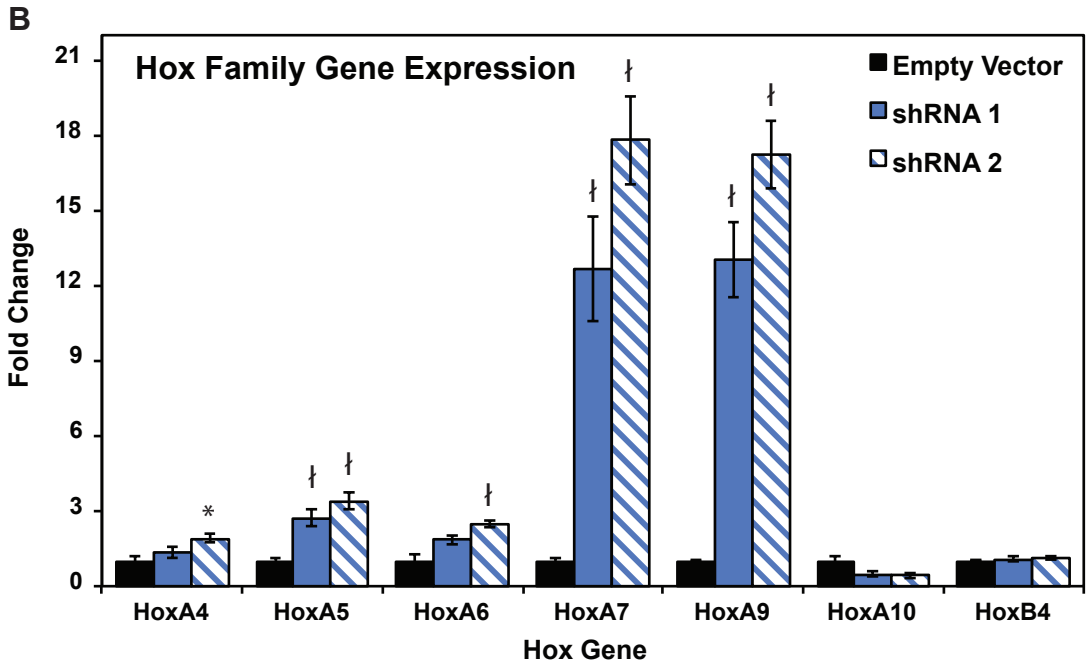
Hox Family Gene Expression
Empty Vector
shRNA 1
shRNA 2
Fold Change
21
18
15
12
9
6
3
0
HoxA4
HoxA5
HoxA6
HoxA7
HoxA9
HoxA10
HoxB4
Hox Gene

Figure S6. *Rad21* depletion increases expression of other genes at the *HoxA* cluster. (A) Map of the *Hoxa* genomic locus showing the 5' to 3' orientation of the *Hoxa10*-*Hoxa4* genes. RNA-seq{Mullenders:2015fi} data is shown in *Rad21*-shRNA or Renilla-shRNA infected HSPCs. (B) RT-qPCR of genes in the *Hoxa* cluster as well as the unrelated *Hoxb4* gene. Each data point represents 6 independent biological replicates. The *Hoxa9* expression data included in panel B is the identical data shown in Figure 2C and was included here for comparison.

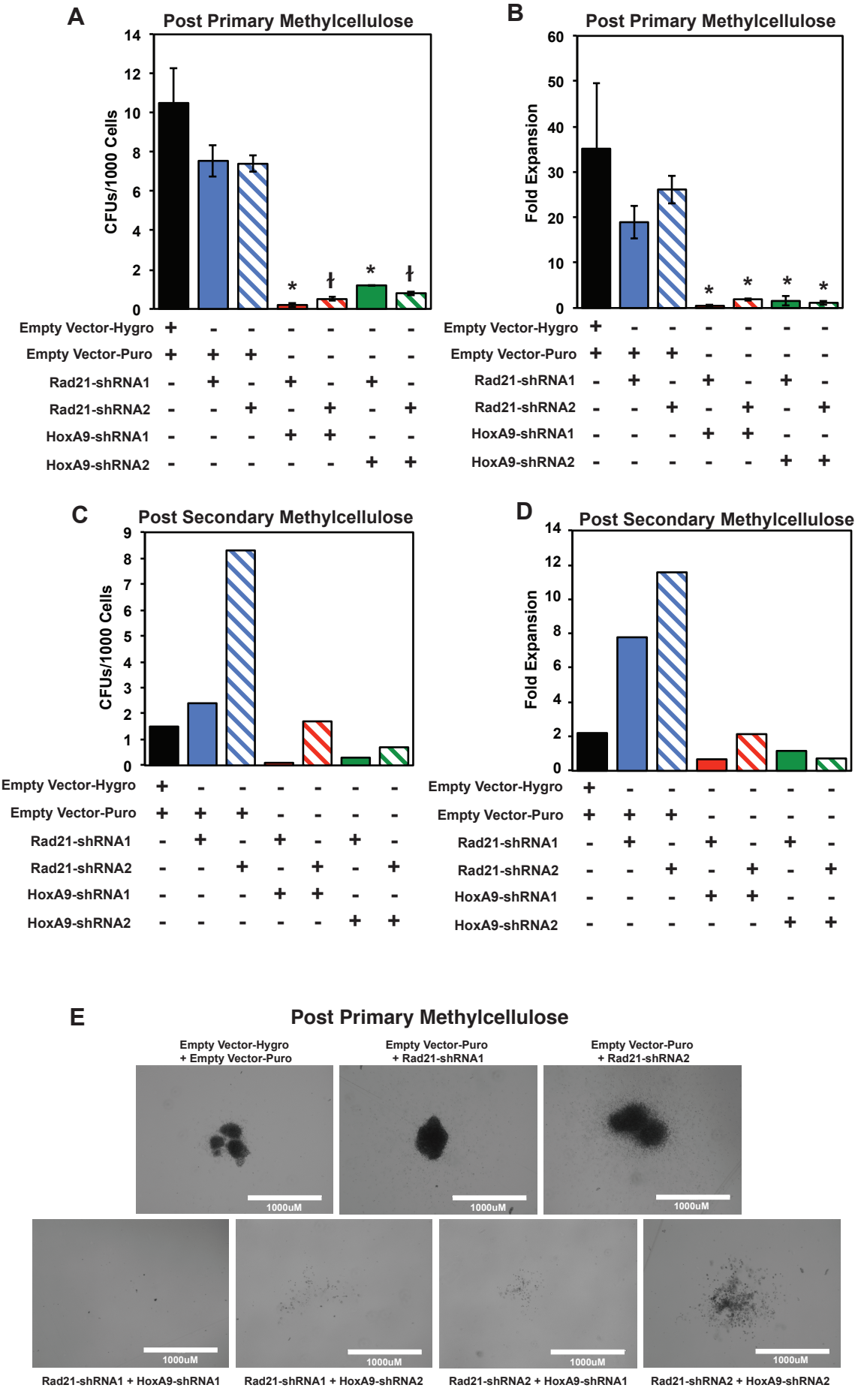
A
Post Primary Methylcellulose
CFUs/1000 Cells
14
12
10
8
6
4
2
0
Empty Vector-Hygro + - - - - - -
Empty Vector-Puro + + + - - - -
Rad21-shRNA1 - + - + - + -
Rad21-shRNA2 - - + - + - +
HoxA9-shRNA1 - - - + + - -
HoxA9-shRNA2 - - - - - + +
B
Post Primary Methylcellulose
Fold Expansion
60
50
40
30
20
10
0
Empty Vector-Hygro + - - - - - -
Empty Vector-Puro + + + - - - -
Rad21-shRNA1 - + - + - + -
Rad21-shRNA2 - - + - + - +
HoxA9-shRNA1 - - - + + - -
HoxA9-shRNA2 - - - - - + +
C
Post Secondary Methylcellulose
CFUs/1000 Cells
9
8
7
6
5
4
3
2
1
0
Empty Vector-Hygro + - - - - - -
Empty Vector-Puro + + + - - - -
Rad21-shRNA1 - + - + - + -
Rad21-shRNA2 - - + - + - +
HoxA9-shRNA1 - - - + + - -
HoxA9-shRNA2 - - - - - + +
D
Post Secondary Methylcellulose
Fold Expansion
14
12
10
8
6
4
2
0
Empty Vector-Hygro + - - - - - -
Empty Vector-Puro + + + - - - -
Rad21-shRNA1 - + - + - + -
Rad21-shRNA2 - - + - + - +
HoxA9-shRNA1 - - - + + - -
HoxA9-shRNA2 - - - - - + +
E
Post Primary Methylcellulose
Empty Vector-Hygro + Empty Vector-Puro
Empty Vector-Puro + Rad21-shRNA1
Empty Vector-Puro + Rad21-shRNA2
1000uM
Rad21-shRNA1 + HoxA9-shRNA1
Rad21-shRNA1 + HoxA9-shRNA2
Rad21-shRNA2 + HoxA9-shRNA1
Rad21-shRNA2 + HoxA9-shRNA2

Figure S7. Co-depletion of *Hoxa9* and *Rad21* blocks HSPC self-renewal. (A-D) Empty vector, *Rad21*-shRNA, and *Rad21*-shRNA+*HoxA9*-shRNA HSPCs were serially passaged in methylcellulose and after each passage colony number (A: post primary and C: post secondary CFUs/1000 cells) and total cell numbers (B: post primary and D: post secondary fold expansion) were determined. (E) Representative images of empty vector, *Rad21*-shRNA, and *Rad21*-shRNA+*HoxA9*-shRNA treated HSPCs at the end of primary plating. Error bars represent standard error of the mean of 2 independent biological replicates. * = $p < 0.05$, ł = $p < 0.01$ vs respective empty vector (IE *Rad21*-shRNA1+empty vector vs *Rad21*-shRNA1+*HoxA9*-shRNA1).

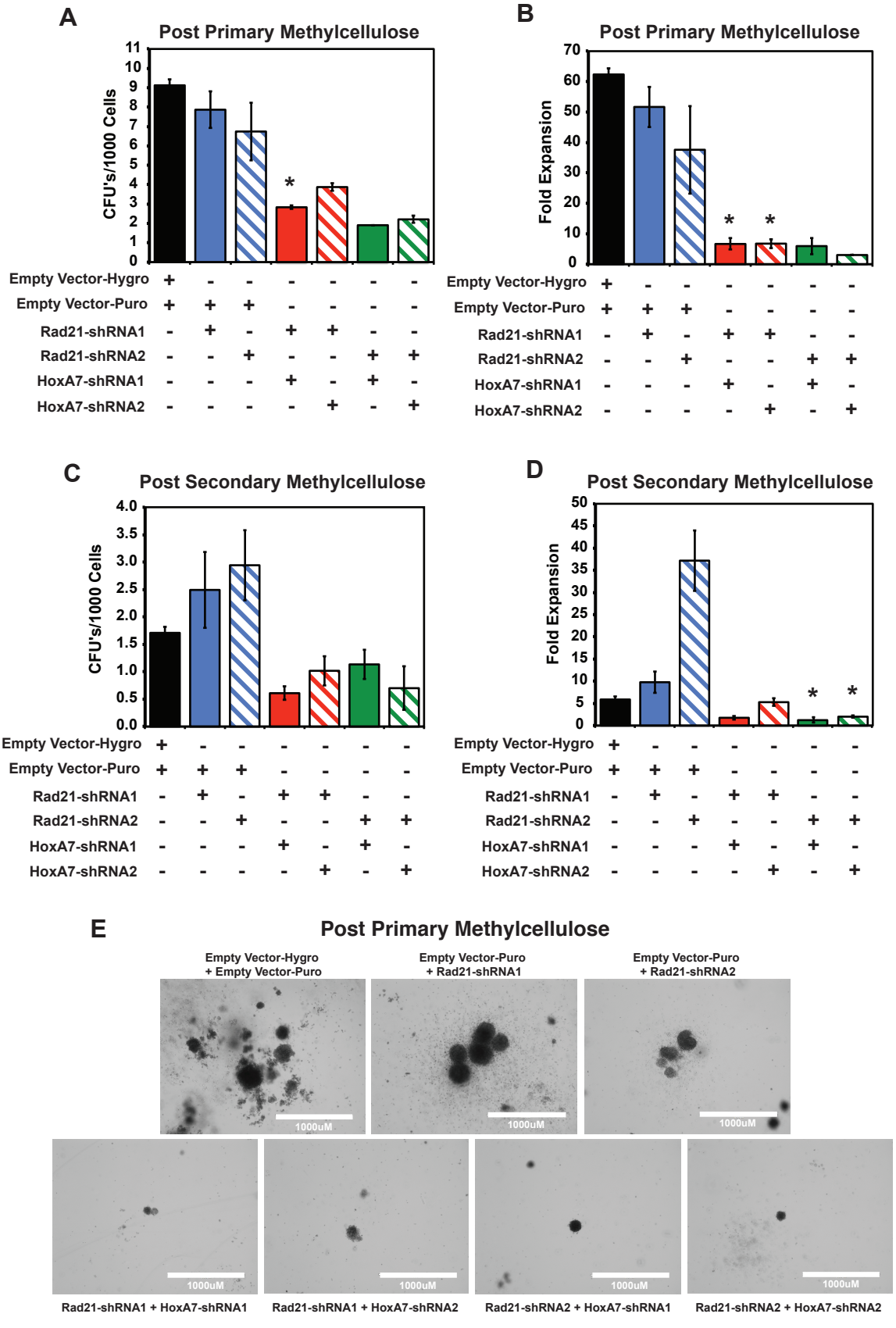
A
Post Primary Methylcellulose
CFU's/1000 Cells
11
10
9
8
7
6
5
4
3
2
1
0
*
Empty Vector-Hygro + - - - - - -
Empty Vector-Puro + + + - - - -
Rad21-shRNA1 - + - + + - -
Rad21-shRNA2 - - + - - + +
HoxA7-shRNA1 - - - + - + -
HoxA7-shRNA2 - - - - + - +
B
Post Primary Methylcellulose
Fold Expansion
70
60
50
40
30
20
10
0
* *
Empty Vector-Hygro + - - - - - -
Empty Vector-Puro + + + - - - -
Rad21-shRNA1 - + - + + - -
Rad21-shRNA2 - - + - - + +
HoxA7-shRNA1 - - - + - + -
HoxA7-shRNA2 - - - - + - +
C
Post Secondary Methylcellulose
CFU's/1000 Cells
4.0
3.5
3.0
2.5
2.0
1.5
1.0
0.5
0.0
Empty Vector-Hygro + - - - - - -
Empty Vector-Puro + + + - - - -
Rad21-shRNA1 - + - + + - -
Rad21-shRNA2 - - + - - + +
HoxA7-shRNA1 - - - + - + -
HoxA7-shRNA2 - - - - + - +
D
Post Secondary Methylcellulose
Fold Expansion
50
45
40
35
30
25
20
15
10
5
0
* *
Empty Vector-Hygro + - - - - - -
Empty Vector-Puro + + + - - - -
Rad21-shRNA1 - + - + + - -
Rad21-shRNA2 - - + - - + +
HoxA7-shRNA1 - - - + - + -
HoxA7-shRNA2 - - - - + - +
E
Post Primary Methylcellulose
Empty Vector-Hygro + Empty Vector-Puro
Empty Vector-Puro + Rad21-shRNA1
Empty Vector-Puro + Rad21-shRNA2
1000uM
Rad21-shRNA1 + HoxA7-shRNA1
Rad21-shRNA1 + HoxA7-shRNA2
Rad21-shRNA2 + HoxA7-shRNA1
Rad21-shRNA2 + HoxA7-shRNA2

Figure S8. Co-depletion of *Hoxa7* and *Rad21* blocks HSPC self-renewal. (A-D) empty vector, *Rad21*-shRNA, and *Rad21*-shRNA+*Hoxa7*-shRNA HSPCs were serially passaged in methylcellulose and after each passage colony number (A: post primary and C: post secondary CFUs/1000 cells) and total cell numbers (B: post primary and D: post secondary fold expansion) were determined. (E) Representative images of empty vector, *Rad21*-shRNA, and *Rad21*-shRNA+*Hoxa7*-shRNA treated HSPCs at the end of primary plating. Error bars represent standard error of the mean of 2 independent biological replicates. * = $p < 0.05$ vs respective empty vector (IE *Rad21*-shRNA1+empty vector vs *Rad21*-shRNA1+*HoxA7*-shRNA1).

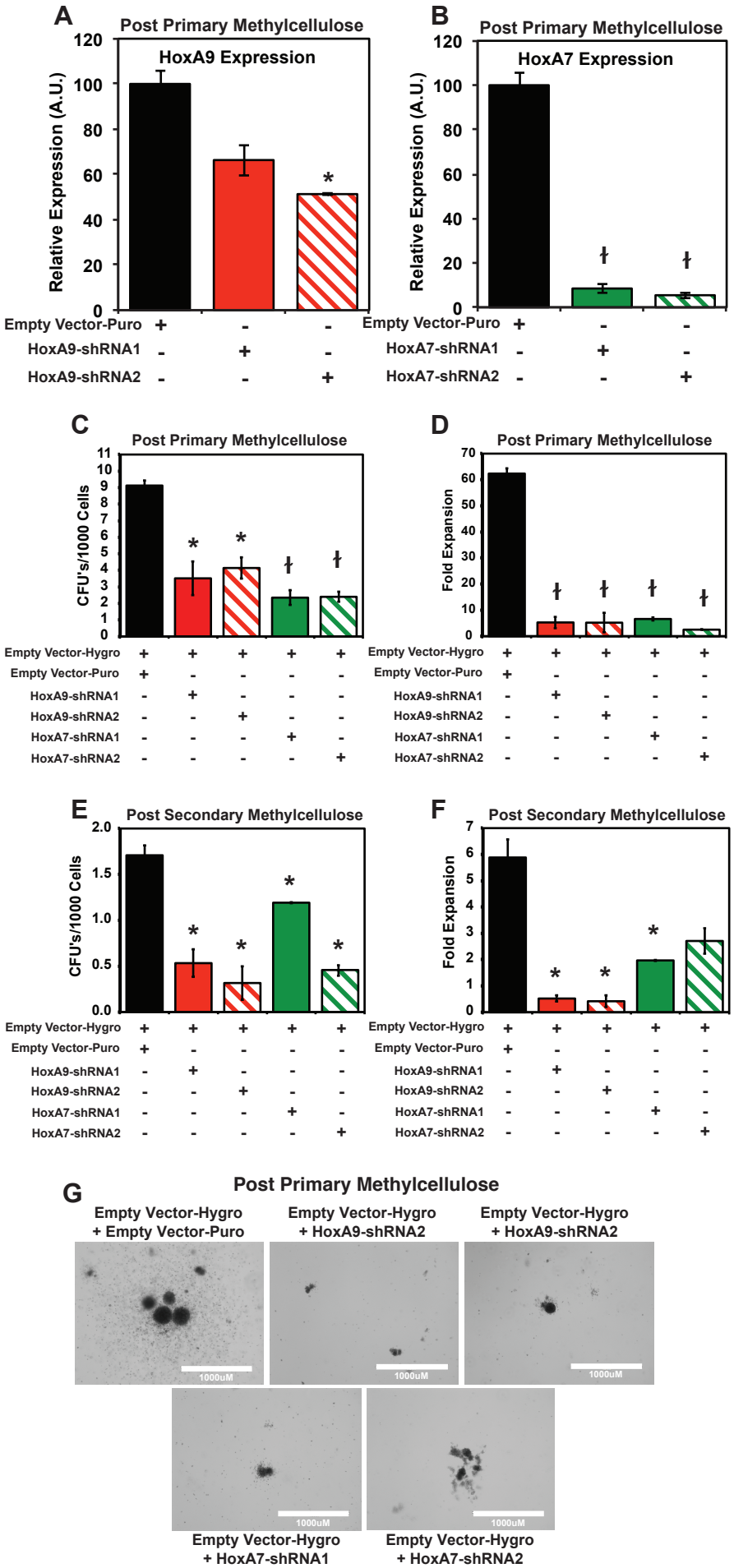
A
Post Primary Methylcellulose
HoxA9 Expression
Relative Expression (A.U.)
120
100
80
60
40
20
0
*
Empty Vector-Puro + - -
HoxA9-shRNA1 - + -
HoxA9-shRNA2 - - +
B
Post Primary Methylcellulose
HoxA7 Expression
Relative Expression (A.U.)
120
100
80
60
40
20
0
†
†
Empty Vector-Puro + - -
HoxA7-shRNA1 - + -
HoxA7-shRNA2 - - +
C
Post Primary Methylcellulose
CFU's/1000 Cells
11
10
9
8
7
6
5
4
3
2
1
0
* * † †
Empty Vector-Hygro + + + + +
Empty Vector-Puro + - - - -
HoxA9-shRNA1 - + - - -
HoxA9-shRNA2 - - + - -
HoxA7-shRNA1 - - - + -
HoxA7-shRNA2 - - - - +
D
Post Primary Methylcellulose
Fold Expansion
70
60
50
40
30
20
10
0
† † † †
Empty Vector-Hygro + + + + +
Empty Vector-Puro + - - - -
HoxA9-shRNA1 - + - - -
HoxA9-shRNA2 - - + - -
HoxA7-shRNA1 - - - + -
HoxA7-shRNA2 - - - - +
E
Post Secondary Methylcellulose
CFU's/1000 Cells
2.0
1.5
1.0
0.5
0.0
* * * *
Empty Vector-Hygro + + + + +
Empty Vector-Puro + - - - -
HoxA9-shRNA1 - + - - -
HoxA9-shRNA2 - - + - -
HoxA7-shRNA1 - - - + -
HoxA7-shRNA2 - - - - +
F
Post Secondary Methylcellulose
Fold Expansion
7
6
5
4
3
2
1
0
* * *
Empty Vector-Hygro + + + + +
Empty Vector-Puro + - - - -
HoxA9-shRNA1 - + - - -
HoxA9-shRNA2 - - + - -
HoxA7-shRNA1 - - - + -
HoxA7-shRNA2 - - - - +
G
Post Primary Methylcellulose
Empty Vector-Hygro + Empty Vector-Puro
Empty Vector-Hygro + HoxA9-shRNA2
Empty Vector-Hygro + HoxA9-shRNA2
1000uM
1000uM
1000uM
1000uM
1000uM
Empty Vector-Hygro + HoxA7-shRNA1
Empty Vector-Hygro + HoxA7-shRNA2

Figure S9. Depletion of *Hoxa7* and *Hoxa9* disrupts self-renewal in control HSPCs. (A) RT-qPCR analysis of *Hoxa7* or *Hoxa9*-depleted HSPCs at the end of primary methylcellulose culture showing shRNA-mediated depletion of *Hoxa7* and *Hoxa9*. (B-E) Empty vector, *Hoxa7*-shRNA, and *Hoxa9*-shRNA treated HSPCs were serially passaged in methylcellulose and after each passage colony number (B: post primary and D: post secondary CFUs/1000 cells) and total cell numbers (C: post primary and E: post secondary fold expansion) were determined. (F) Representative images of empty vector, *Hoxa7*-shRNA, and *Hoxa9*-shRNA treated HSPCs at the end of primary plating. The empty vector-puro+empty vector-hygro data points in panels A-D are identical to those shown in Figure S7A-D and were included here for comparison. Error bars represent standard error of the mean of 2 independent biological replicates.

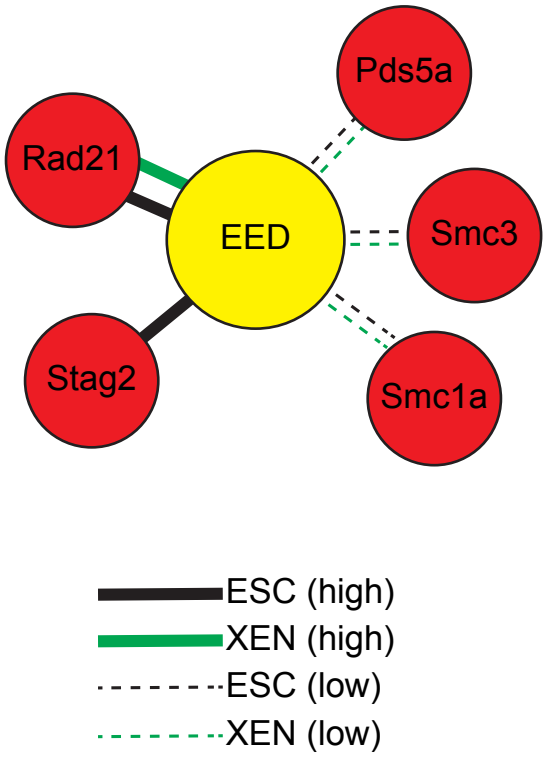
Pds5a
Rad21
EED
Smc3
Stag2
Smc1a
ESC (high)
XEN (high)
ESC (low)
XEN (low)

Figure S10. Rad21 interacts with members of the PRC2 complex. Proteomic analysis indicating that the PRC2 subunit Eed directly interacts with members of the cohesin complex. Data were reanalyzed from {Cao:2014ki}. Interactions between Eed and cohesin complex members (including Rad21) were identified in both embryonic stem cells (ES) and extraembryonic endoderm (XEN) cells.

Mouse ENCODE Data

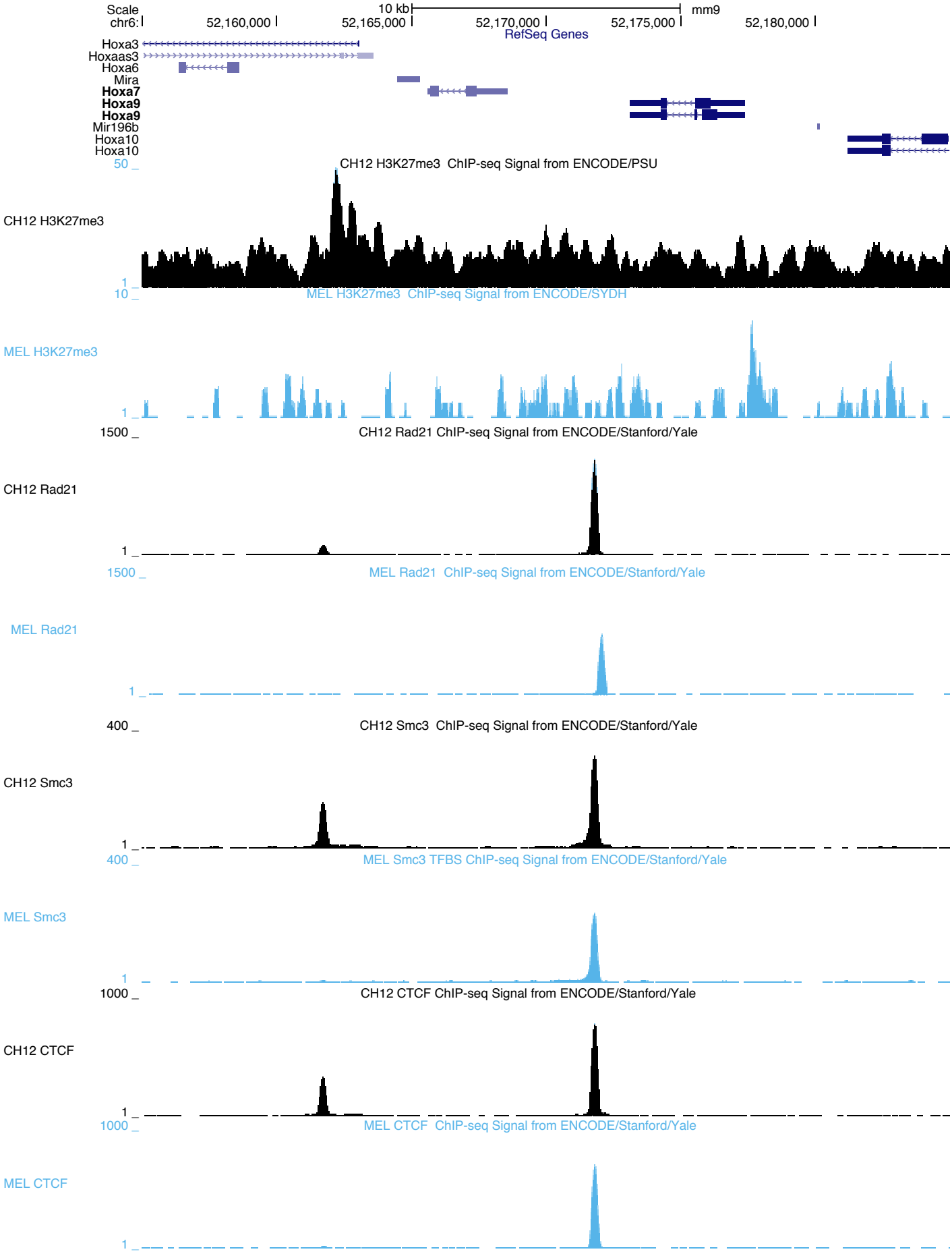

Figure S11. Cohesin occupies the *Hoxa9* locus in murine cells. Data from the ENCODE project was reanalyzed to monitor cohesin occupancy at the *Hoxa9* locus. Tracks show cohesin and Ctcf peaks located within the murine *Hoxa9* locus in murine erythroleukemia cells (MEL) and lymphoma (CH12) cell lines. Tracks for histone H3K27me3, Rad21, Smc3, and Ctcf are shown for each. For all tracks, the Y-axis scale is the same for each factor in the different cell lines, with the exception of H3K27me3.

Human ENCODE

Figure S12. Cohesin occupies the *HOXA9* locus in human cells. Data from the ENCODE project was reanalyzed to monitor cohesin occupancy at the *HOXA9* locus. Tracks show cohesin and CTCF peaks located within the human *HOXA9* locus in myeloid leukemia cells (K562) and hepatocellular carcinoma (HepG2) cells. Tracks for histone H3K27me3, RAD21, EZH2, and CTCF are shown for each. For all tracks, the Y-axis scale is the same for each factor in the different cell lines.

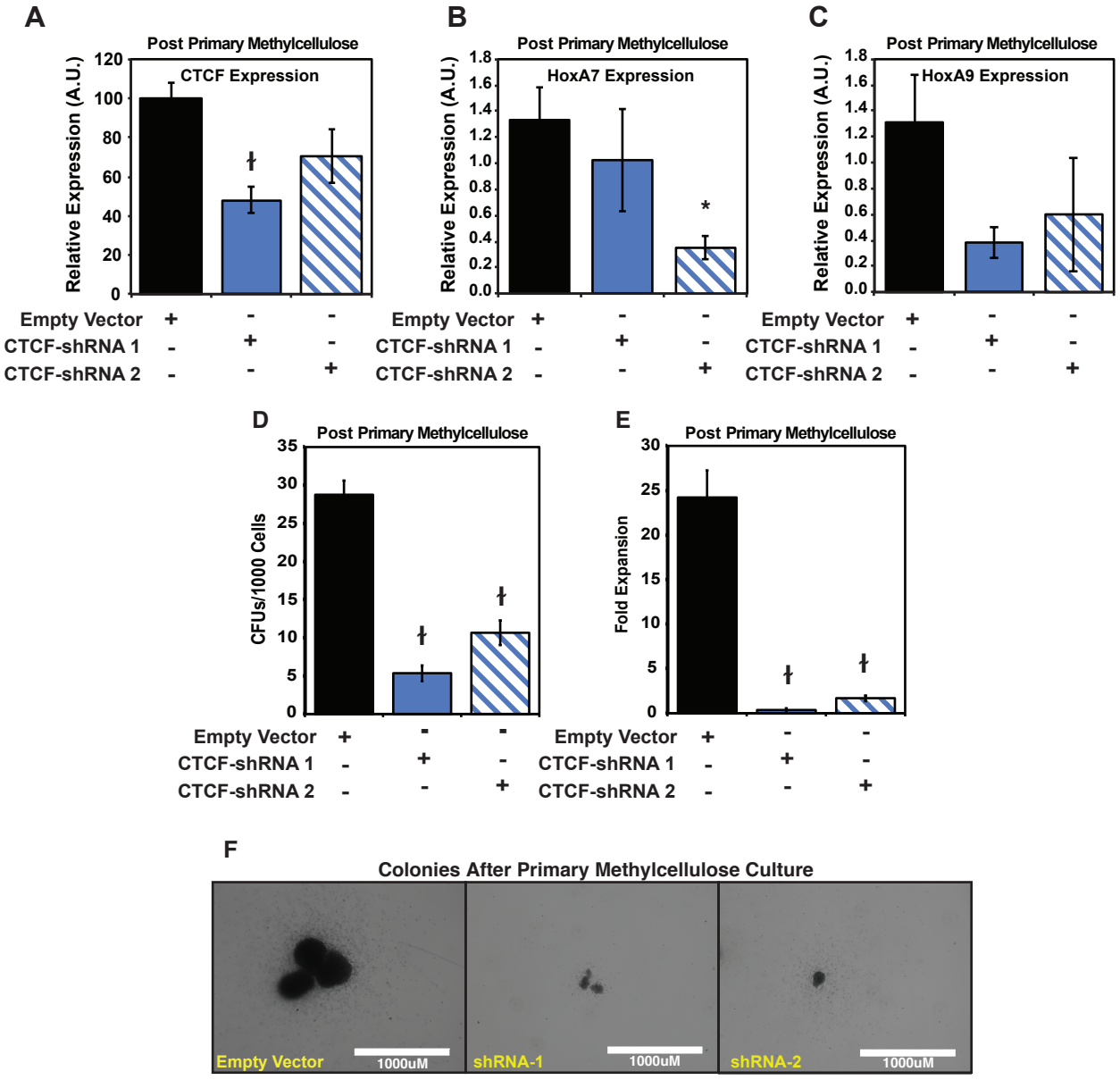
A
Post Primary Methylcellulose
CTCF Expression
Relative Expression (A.U.)
120
100
80
60
40
20
0
Empty Vector + - -
CTCF-shRNA 1 - + -
CTCF-shRNA 2 - - +
B
Post Primary Methylcellulose
HoxA7 Expression
Relative Expression (A.U.)
1.8
1.6
1.4
1.2
1.0
0.8
0.6
0.4
0.2
0.0
*
Empty Vector + - -
CTCF-shRNA 1 - + -
CTCF-shRNA 2 - - +
C
Post Primary Methylcellulose
HoxA9 Expression
Relative Expression (A.U.)
1.8
1.6
1.4
1.2
1.0
0.8
0.6
0.4
0.2
0.0
Empty Vector + - -
CTCF-shRNA 1 - + -
CTCF-shRNA 2 - - +
D
Post Primary Methylcellulose
CFUs/1000 Cells
35
30
25
20
15
10
5
0
Empty Vector + - -
CTCF-shRNA 1 - + -
CTCF-shRNA 2 - - +
E
Post Primary Methylcellulose
Fold Expansion
30
25
20
15
10
5
0
Empty Vector + - -
CTCF-shRNA 1 - + -
CTCF-shRNA 2 - - +
F
Colonies After Primary Methylcellulose Culture
Empty Vector
1000uM
shRNA-1
1000uM
shRNA-2
1000uM

Figure S13. Depletion of *Ctcf* does not enhance HSPC self-renewal nor alter *Hoxa7* or *Hoxa9* expression. (A-C) RT-qPCR analysis of empty vector, or *Ctcf*-shRNA treated HSPCs the end of primary methylcellulose culture showing shRNA-mediated *Ctcf* depletion (A), and *Hoxa7* (B) and *Hoxa9* (C) expression. (D+E) Empty vector, *and* *Ctcf*-shRNA treated HSPCs were cultured in methylcellulose and at the end of primary passage, colony number (D; CFUs/1000 cells) and total cell numbers (E: fold expansion) were determined. (F) Representative images of empty vector, and *Ctcf*-shRNA treated HSPCs at the end of primary plating. Error bars represent standard error of the mean of 4 independent biological replicates.

Supplemental Tables:

Table S1: List of all qPCR primers used in these studies

Table S2: List of all antibodies used in these studies

Table S3: List of all publicly available datasets reanalyzed for this manuscript

Table S4: Transcript abundance in FPKM (Fragment per Kilobase per Million reads) for well-annotated RefSeq protein coding genes. Original data derived from{Mullenders:2015fi}.

Table S5: Microarray data from cells infected with an empty vector or two different shRNAs to *Rad21* at the end of primary passage.

Table S6: All gene sets enriched (p-value<0.01, FDR<25%) in *Rad21* depleted cells from GSEA.

Author Contributions:

The majority of experiments were performed by JF, JP, MR and CS. ZJG performed co-immunoprecipitation experiments, AMA assisted with flow cytometry approaches. KP and SR performed transcriptome analyses. JMS and CS analyzed TCGA data. MM, S. Malarkanna, JDC, and S. Milanovich assisted with the design and interpretation of the studies. All authors assisted with drafting and revising the manuscript, and approved with submission of the manuscript. S.Rao as corresponding author had full access to all raw data contained within this manuscript.

Acknowledgements:

S. Malarkannan is supported by NIH R01 AI102893, NCI R01 CA179363, HRHM Program of the MACC Fund, Nicholas Family Foundation; Gardetto Family Foundation; J. Crispino is supported by the Heartland Blood Centers and NIH R01 CA101774; M. McNulty is supported as a trainee of T32CA009560; S. Milanovich is supported by grants from National Institute of General Medical Sciences: NIH grant 5P20GM103548-5, and the MACC Fund.